Single-Stage Fractionation of Poly(Ethylene-co-Vinyl Acetate) in Supercritical Ethylene with SAFT

Bernard Folie
Exxon Chemical Company, Baytown Polymers Center, Baytown, TX 77522

Using the discrete thermodynamics approach, the single-stage fractionation of a polydisperse poly(ethylene-co-vinyl acetate) in supercritical ethylene and ethylene-vinyl acetate mixtures is modeled with an EOS rooted in statistical associating fluid theory (SAFT). The simulation results are compared to new high-pressure coexistence data and size-exclusion chromatography data obtained on a few selected extracts. The polymer molecular-weight distribution is optimally represented by ten nearly-monodisperse pseudocomponents, determined by a nonuniform lumping method. SAFT quantitatively captures the effect of pressure, temperature and solvent composition on the solvent capacity and the extract yield over a broad range of conditions. The ethylene capacity monotonically increases with increasing pressure between 200 bar and the cloud point pressure, with increasing VA concentration in the solvent mixture, and with increasing temperature above ~ 480 bar. At intermediate pressure (200 – 480 bar), SAFT predicts that the ethylene capacity behaves nonmonotonically with temperature. The extract and raffinate molecular weight and polydispersity are predicted also from SAFT as a function of pressure and solvent composition for a typical bubble- and dew-point-type fractionation, thereby illustrating the underlying differences between those two phase disengagement mechanisms.

Introduction

Poly(ethylene-co-vinyl acetate) (EVA) is a statistical copolymer of ethylene and vinyl acetate (VA), produced commercially by free-radical polymerization in the high-pressure polyethylene (HPPE) process. In this process, it is sometimes desirable to carry out the bulk polymerization reaction in a two-phase region by changing the pressure and/or the temperature to cross the fluid → fluid-liquid phase transition (Folie and Radosz, 1995; Bogdanovic et al., 1981, 1985). The amount and composition of each of the two phases formed will affect the polymerization kinetics, hence the final properties of the product, since the solubility of the monomers, the free-radical initiators, and the chain-terminating agents differ in both phases (Bogdanovic et al., 1981, 1985). Downstream of the polymerization, the product is separated from the bulk of the unreacted monomers by lowering the pressure in the fluid-liquid region, with ethylene acting as a supercritical antisolvent for the polymer at typical separation conditions (Folie and Radosz, 1995). Since the low-density polyethylenes (LDPEs) manufactured in the HPPE process are always characterized by a broad molecular-weight distribution (MWD), they undergo fractionation during the supercritical separation step whereby the light ends are extracted in the polymer-lean phase (PLP) while the bulk of the polymer is contained in the polymer-rich phase (PRP). In order to optimize the two-phase polymerization process and/or the supercritical separation in the HPPE process, it is crucial to estimate the phase compositions (coexistence points), the relative amount of each phase formed, and the physical properties (such as molecular weight and polydispersity) of the polymer in each phase over a wide range of pressures, typically from 200 bar to the cloud point pressure (CPP). Such estimates can be made using an equation of state (EOS) applicable to polymer-supercritical fluid systems coupled to a flash algorithm. Among the EOSs developed for polymer systems such as the free-volume models, the lattice-fluid models, and the continuum models such as SAFT, the continuum models are usually the most effective for process design purposes because they are applicable over a wide range of densities (from low-pressure gases to compressed liquids) and molecular weights (from small to large molecules), and are easy to extend to mixtures (Wohlfarth, 1993).

Although many experimental cloud point data are avail-

able from the literature for ethylene solutions of LDPE homo- and copolymers (recently reviewed by Folie and Radosz, 1995), coexistence data for these systems are sparse. Two important references in this area are the early work by Luft (Luft and Lindner, 1976; Spahl and Luft, 1983) for the LDPE-ethylene system and, more recently, by Finck et al. (1992) for the EVA-ethylene-VA system. Similarly, whereas many studies have focused on modeling the high-pressure phase equilibria of these systems by treating the polymer as a monodisperse component, comparatively few have taken the polymer polydispersity into account. It is well-known since the early work of Koningsveld and Staverman (1968) and Flory (1990) among others that the phase equilibria of polymer solutions are strongly affected by the polymer polydispersity. For example, the size of the fluid-liquid miscibility gap and the polymer solubility in the PLP can be largely underestimated by treating the polymer as a monodisperse component with an average MW. Bonner et al. (1974), then Bogdanovic et al. (1981, 1985), used an EOS based on the free-volume theory of Flory and Prigogine to model the high-pressure phase equilibria of a LDPE in ethylene. Ratzsch et al. (1983) also used the free-volume theory and the continuous thermodynamics approach to study the effect of polydispersity on the phase equilibria of EVA in ethylene. Later, the same LDPE-ethylene system was modeled by Liu and Prausnitz (1980) and Jungermann and Luft (1987) using an EOS based on the perturbed-hard chain theory, and by Sako et al. (1989) who developed a simple cubic EOS from the generalized van der Waals partition function.

More recently, the SAFT EOS was used with success by McHugh (Lee et al., 1994) and by Folie et al. (1996) to model the cloud point curves of LDPE copolymers including EVA and poly(ethylene-co-methyl acrylate) (EMA) in supercritical ethylene. In those studies, the polymer was always treated as a monodisperse component. Chen et al. (1993, 1994a) used SAFT to quantify staging effects on the fractionation of linear polyethylene in supercritical ethylene and 1-hexene. In their work, six arbitrarily-chosen pseudocomponents were used to mimic the polydispersity effect. In another application area, SAFT was used by Bolanos and Thies (1995) to correlate liquid-liquid coexistence data obtained for supercritical toluene-petroleum pitch mixtures.

In this work, the single-stage fractionation of a commercial EVA, characterized by a broad MWD but a narrow chemical composition distribution, in supercritical ethylene and ethylene-VA mixtures is modeled with the SAFT EOS coupled to a block-algebra flash algorithm developed for large multicomponent systems (Chen et al., 1993, 1994a). The polymer MWD, measured by size-exclusion chromatography (SEC), is represented by a finite number of nearly-monodisperse pseudocomponents obtained from a nonuniform lumping method. SAFT is used to predict the solvent capacity, the extract yield, and the relative amount of each phase formed over a broad range of pressures (200 bar to the CPP), temperatures (130–250°C), and solvent compositions. The SAFT predictions are compared to new high-pressure coexistence data obtained for supercritical solutions of EVA in ethylene and ethylene-VA mixtures containing up to 50 wt. % VA in the solvent mixture. Last, SAFT is used to predict the average MW and polydispersity of the polymer in both phases for a typical bubble and dew-point-type fractionation. The SAFT simulation results are compared to SEC data obtained on a few selected extracts.

Experimental Procedure

The phase equilibrium measurements were carried out in a well-thermostated 0.75-L autoclave designed to sustain pressures up to 2,500 bar and temperatures up to 250°C. The equipment and experimental procedure are described in detail elsewhere (Luft and Subramanian, 1987). Briefly, the cloud-point phase transitions were observed visually through illuminated sapphire windows. The cloud point was determined by gradually lowering the pressure at constant temperature and composition until the initially-clear solution became turbid. Next, the composition of the phases in equilibrium was determined by sampling each phase through needle valves mounted at the top and bottom of the autoclave. The samples were collected in flasks cooled with liquid nitrogen. After weighing, each sample was separated into ethylene, VA, and polymer by evaporation. The amount of polymer was determined gravimetrically, whereas the relative amounts of ethylene and VA were determined by gas chromatography.

SEC was performed at 135°C on a Waters 150-C ALC/GPC equipped with a Waters Differential Refractive Index (DRI) detector. The samples are typically prepared at a concentration of 3.5 mg per mL in 1,2,4-trichlorobenzene. HPLC-grade 1,2,4-trichlorobenzene, to which 0.1 vol. % of polyethylene glycol is added, is also used as the eluting solvent (0.5 mL/s). The samples are separated according to their hydrodynamic volume over four Shodex columns, packed with styrene-divinylbenzene gels. The refractometer was calibrated with polystyrene standards and the calibration curve corrected for the presence of 18 wt. % VA incorporated in the polymer backbone (determined by ^{1}H-NMR). SEC was performed to determine the MWD of the parent EVA and of a few selected extracts, from which their weight-average MW (M_w), number-average MW (M_n), and polydispersity ($= M_w/M_n$) were estimated.

Selection of Pseudocomponents

One of the key challenges in modeling the fractionation of a polydisperse polymer by the discrete thermodynamics approach is the selection of the polymer pseudocomponents. The pseudocomponents are obtained by grouping molecules of similar size by an appropriate lumping method. The average MW and the relative weight fraction of each pseudocomponent are determined for the multicomponent phase equilibrium calculations. On the one hand, the number of pseudocomponents needs to be large enough to accurately represent the characteristic shape of the polymer MWD. On the other hand, one would like to minimize the number of pseudocomponents to reduce the computational time required for the multicomponent flash calculations.

In this work, we use a nonuniform lumping method recommended by Huang and Radosz (1991b, 1991c) for non-Gaussian, asymmetrically distributed systems. The essence of their method is to map the original distributed variable (M_i) with a logarithmic lumping function $F = \log_{10}(M_i)$, discretize the

function domain into k equal segments, and re-map the distributed variable into its original domain according to

$$M_i = F^{-1}\left\{F(M_0) + i\left[\frac{F(M_k) - F(M_0)}{k}\right]\right\} \quad \text{for} \quad i = 0 \text{ to } k \tag{1}$$

from which the average MW ($M_{i,\text{mid}}$) of the ith pseudocomponent is taken as the arithmetic average (midpoint) of the interval $[M_{i-1}, M_i]$:

$$M_{i,\text{mid}} = (M_{i-1} + M_i)/2 \tag{2}$$

This method generates segments of increasing size length in the original M_i domain bounded by $[M_0, M_k]$: $M_0M_1 < M_1M_2 < \ldots < M_{k-1}M_k$. This way, if M_0 is the low MW bound, the light ends are more finely divided than the heavy ends. If, on the contrary, M_0 is the high MW bound, the heavy ends are finely divided and the light ends coarser. Since the main objective of this work is to predict the solubility of the light ends in supercritical ethylene, we set M_0 equal to the low MW bound, $M_0 = 1.1$ kg/mol, and $M_k = 870$ kg/mol.

One method to estimate the relative weight fraction of each pseudocomponent is to curve fit the MWD data with some suitable probability density function from which the weight fraction of the ith pseudocomponent can be estimated by numerically computing the area under the curve in the interval $[M_{i-1}, M_i]$. In this work, we use a discrete method which does not require curve fitting. Since the signal obtained from the DRI detector is made of discrete data points (DRI_i) obtained at a fixed sampling time interval, we normalize these data ($p_{w_i} = DRI_i/\Sigma DRI_i$) to obtain a discrete weight probability distribution for M_i ($\Sigma p_{w_i} = 1$). By cumulating probabilities (p_{w_i}), we obtain the cumulative weight probability distribution from which the weight fraction of the ith pseudocomponent is easily obtained from

$$w_i = Cw_i - Cw_{i-1} \tag{3}$$

where the cumulative weight probabilities (Cw_is) are estimated by interpolating between the data points with cubic splines. It should be pointed out that an elegant method, the so-called generalized Gaussian quadrature method, developed by Cotterman and Prausnitz (1985) and used elsewhere (Kang and Sandler, 1988; Kang et al., 1989), exists for estimating the pseudocomponents in a mathematically correct and optimal way, given a continuous distribution function for M_i.

Two sets of criteria are used to determine the optimum number of pseudocomponents. First, the reconstructed EVA M_w and M_n are calculated according to

$$M_w = \sum_{i=1}^{k} (w_i M_{i,\text{mid}}) \tag{4}$$

and

$$\frac{1}{M_n} = \sum_{i=1}^{k} (w_i / M_{i,\text{mid}}) \tag{5}$$

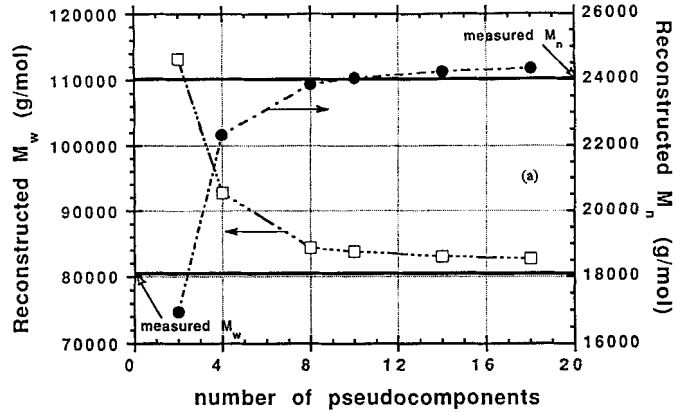

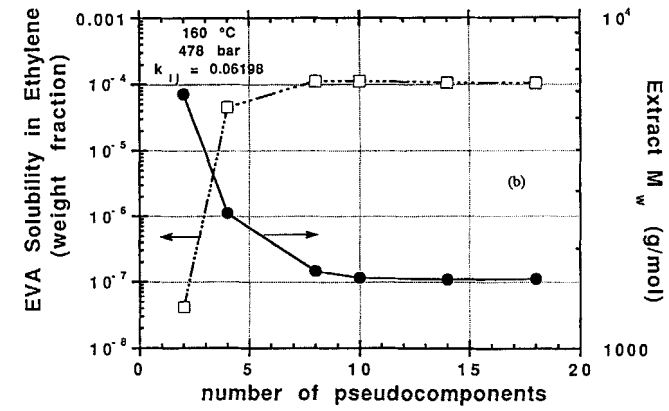

Figure 1. (a) Reconstructed M_w and M_n of parent EVA as function of number of pseudocomponents; (b) EVA solubility in supercritical ethylene and extract M_w, calculated from SAFT at 160°C and 478 bar, as function of number of pseudocomponents.

and compared to the experimentally-determined values obtained from SEC. The results are shown in Figure 1a. Clearly, both reconstructed MWs asymptotically approach the measured values as the number of pseudocomponents increases. When the number of pseudocomponents is ten, the reconstructed M_n (24,080 g/mol) is nearly equal to the measured M_n (24,040 g/mol), whereas the reconstructed M_w (83,810 g/mol) is slightly larger than the measured M_w (80,520 g/mol). From this first set of criteria, we choose ten as the optimum number of pseudocomponents since M_n measured by SEC-DRI is generally more accurate than M_w for nonlinear chain molecules.

As stated, the main objective of this work is to predict the light ends solubility in supercritical ethylene. Hence, we use as the second set of criteria the solubility of EVA in ethylene and the extract M_w calculated from SAFT at a constant pressure of 478 bar and a constant temperature of 160°C. The results are presented in Figure 1b. Clearly again, both calculated variables asymptotically reach a constant value when the number of pseudocomponents approaches ten. The reconstructed MWD obtained with ten pseudocomponents is

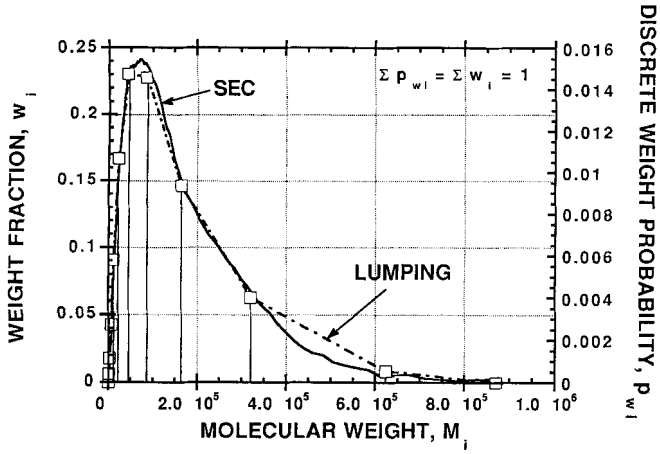

Figure 2. Molecular-weight distribution (MWD) of parent EVA.

Solid curve is MWD measured by SEC, while dashed curve represents MWD reconstructed from ten pseudocomponents obtained from nonuniform lumping method.

shown in Figure 2 where it is compared to the experimentally-determined MWD. The agreement between the two distributions is satisfactory. The properties of the pseudocomponents are summarized in Table 1. Interestingly, all the ten pseudocomponents are nearly-monodisperse, $(M_w/M_n)_i < 1.05$.

Statistical Associating Fluid Theory

SAFT is a molecularly-based EOS that incorporates terms accounting for the molecular size and shape (such as chain length and branchiness), association (such as hydrogen bonding) energy, and mean-field (such as dispersion) energy. SAFT development, approximations, and tests against molecular simulation data are described elsewhere (Chapman et al., 1990; Banaszak et al., 1993; Huang and Radosz, 1990). SAFT was applied to many real pure components (Huang and Radosz, 1990) and fluid mixtures (Huang and Rodosz, 1991a; Hasch et al., 1994), including supercritical and near-critical solutions of polymers, such as alternating poly(ethylene-co-propylene) (PEP) and polyisobutylene (PIB). For example, SAFT was found to account for phase transitions in binary and ternary systems of PEP-α-olefin (Gregg et al., 1993), PVT data for pure PEP systems (Chen et al., 1994b), and for the associating effects in binary systems of monohydroxyl and dihydroxy telechelic PIB in nonpolar and polar solvents (Gregg et al., 1994).

Table 1. Average MW and Polydispersity of Pseudocomponents and Parent EVA

Pseudo-component	$M_{i,\mathrm{mid}}$ (g/mol)	w_i	PD_i^*
EVA1	1,560	0.0063	1.027
EVA2	3,040	0.0178	1.034
EVA3	5,910	0.0426	1.038
EVA4	11,490	0.0906	1.034
EVA5	22,360	0.1669	1.040
EVA6	43,500	0.2306	1.032
EVA7	84,650	0.2278	1.040
EVA8	164,700	0.1464	1.034
EVA9	320,450	0.0627	1.031
EVA10	623,500	0.0083	1.027
Parent EVA	M_w (g/mol)	M_n (g/mol)	PD^*
Measured by SEC	80,520	24,040	3.35
Reconstructed (10 pc)	83,810	24,080	3.48
Reconstructed** (8 pc)	104,090	24,320	4.28

*PD is the polydispersity = M_w/M_n.
**Calculated by lumping the last three pseudocomponents (EVA8, EVA9, and EVA10) into one single pseudocomponent.

A SAFT fluid is a collection of spherical segments that are not only exposed to repulsive (hard-sphere) and attractive (dispersion) forces, but can also aggregate through covalent bonds to form chains (chain effect), and through hydrogen bonds to form short-lived clusters (association effect). The reference part of SAFT includes the hard-sphere, chain, and association terms. The perturbation part accounts for the relatively weaker, mean-field dispersion-like effects. The SAFT residual Helmholtz free energy (A^{res}) relative to an ideal gas reference state is given by

$$A^{\mathrm{res}} = A^{\mathrm{ref}} + A^{\mathrm{disp}} \tag{6}$$

with

$$A^{\mathrm{ref}} = A^{\mathrm{hs}} + A^{\mathrm{chain}} + A^{\mathrm{assoc}} \tag{7}$$

In order to extend SAFT to real fluids, one needs three pure component parameters for nonassociating fluids: u^0 the temperature-independent segment-segment interaction energy; v^{00} the temperature-independent segment volume; and m the segment number. Also needed are two association parameters that characterize each site-site interaction: ϵ the energy of association between sites on a molecule; and κ the reduced volume of association. The association term in Eq. 7 is typically used in systems with hydrogen-bonding molecules (Gregg et al., 1994). Hence, it was set to zero in this work ($A^{\mathrm{assoc}} = 0$).

The three pure component parameters u^0, v^{00}, and m for both monomers (ethylene and VA) are found by fitting SAFT to pure component vapor pressures and saturated liquid densities, as described elsewhere (Huang and Rodosz, 1990, 1991a). The pure component parameters for the ten nearly-monodisperse EVA pseudocomponents were estimated as detailed by Folie et al. (1996). Following Huang and Rodosz (1990), we set v^{00} equal to 12 mL/mol-seg, and estimate m and u^0/k from the n-alkane corollaries

$$m = 0.05096 M_{i,\mathrm{mid}} \tag{8}$$

and

Recently, SAFT was successfully used to model the cloud points of EVA in supercritical ethylene and ethylene-VA mixtures (Folie et al., 1996). SAFT was found to account for the effect of the polymer MW and VA content, and solvent composition on the CPP and on the size of the fluid-liquid miscibility gap over a broad range of temperatures and polymer concentrations. Although the copolymer was treated as a monodisperse component in those simulations, quantitative agreement with experimental data was obtained in most instances.

Table 2. SAFT Pure Component Parameters for Solvents and Pseudocomponents

Component	MW (g/mol)	m	v^{00} (mL/mol-seg)	u^0/k (K)
Ethylene	28.054	1.464	18.157	212.06
VA	86.091	5.723	6.948	191.93
EVA_i	$M_{i,\mathrm{mid}}$	$0.05096 \times M_{i,\mathrm{mid}}$	12.00	210.00

$$u^0/k = 210 - 26.886 \exp(-0.013341 M_{i,\mathrm{mid}}) \qquad (9)$$

where $M_{i,\mathrm{mid}}$ stands for the average MW of the ith pseudocomponent as given by Eq. 2 and k is the Boltzmann's constant. For high MW polymers, Eq. 9 is equivalent to using a constant u^0/k value of 210 K. The SAFT parameters used for ethylene, VA, and the ten pseudocomponents are summarized in Table 2.

In order to extend SAFT to real fluid mixtures, mixing rules are required only for the dispersion term since the three reference terms can be extended to mixtures based on rigorous statistical mechanics. The van der Waals one-fluid (vdW1) mixing rules are used for the two parameters in the dispersion term that require mixing rules, u/k, the temperature-dependent segment-segment interaction energy, and m. As explained elsewhere (Folie et al., 1996), only one binary interaction parameter k_{ij} per pair of components was used in this work. k_{ij} is a correction factor to the geometric mean rule used to estimate the unlike-segment interaction energy u_{ij} which appears in the vdW1 mixing rule for u/k

$$u_{ij} = (1 - k_{ij})(u_{ii} u_{jj})^{1/2} \qquad (10)$$

For an n-component system, the number of k_{ij}s ideally required is equal to $(n^2 - n)/2$ if $k_{ij} = k_{ji}$ and $k_{ii} = 0$. According to this rule, 66 k_{ij}s are required for the 12-component system of this work, which is obviously impractical. In fact, this number can be reduced to a convenient set of three k_{ij}s by assuming that the k_{ij}s between the EVA pseudocomponents and the solvents are equal to those between the parent EVA and the solvents, and by setting the k_{ij} between any two EVA pseudocomponents equal to zero. These assumptions can be rationalized by recognizing that: (i) ideally, the k_{ij}s ought to be MW-independent; (ii) VA is randomly and uniformly distributed on the polymer chains, independently of their size. Hence, only three k_{ij}s were used in this work: one for the ethylene-VA interaction (k_{12}), one for the ethylene-EVA interaction (k_{13}), and one for the VA-EVA interaction (k_{23}). These k_{ij}s were determined by Folie et al. (1996) by fitting SAFT to vapor-liquid equilibrium (VLE) data for the ethylene-VA binary, and to cloud point data for the parent EVA-ethylene pseudo-binary and the parent EVA-ethylene-VA pseudo-ternary systems. Furthermore, since all three k_{ij}s were found to be only slightly dependent upon temperature, three temperature-independent k_{ij}s were used throughout this work: $k_{12} = 0.15340$, $k_{13} = 0.06198$, and $k_{23} = 0.08583$.

Results and Discussion

Solvent capacity

The effect of pressure, temperature, and VA concentration in the solvent mixture on the ethylene capacity is illustrated in Figures 3 to 6. In what follows the *solvent capacity* is defined as the polymer solubility (in weight fraction) in the PLP. The experiments and simulations were performed with ~15 wt. % EVA in the feed. As it will be detailed later, this fractionation is of the bubble-point-type.

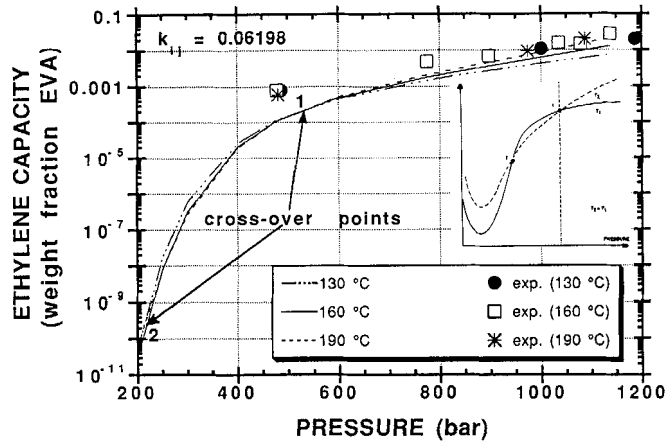

Figure 3. Ethylene capacity shown as three isotherms as function of pressure.

Continuous curves represent SAFT predictions while points are experimental coexistence data collected in this work.

The effect of pressure and temperature on the ethylene capacity is illustrated by the three isotherms shown in Figure 3. The agreement between the experimental data and the SAFT simulations (the continuous curves) is relatively good considering the wide pressure range (200 – 1,200 bar) over which the simulations were performed. The shape of those isotherms is typical for solute-SCF systems. The solvent capacity decreases monotonically with pressure, slowly at first, and then more steeply as the pressure approaches the critical pressure of ethylene ($P_c = 50.4$ bar). The effect of temperature on the solvent capacity is nonmonotonic as indicated by the presence of two crossover points (labeled 1 and 2 in Figure 3) where the 130°C and 190°C isotherms cross each other. At high pressures ($P >$ ~480 bar), the solvent capacity is controlled by energy-related effects; hence, it increases with increasing temperature. At intermediate pressures (~200

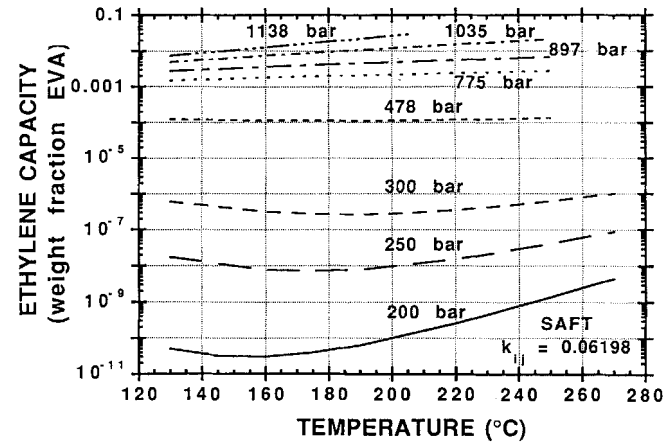

Figure 4. Ethylene capacity predicted by SAFT shown as isobars as function of temperature.

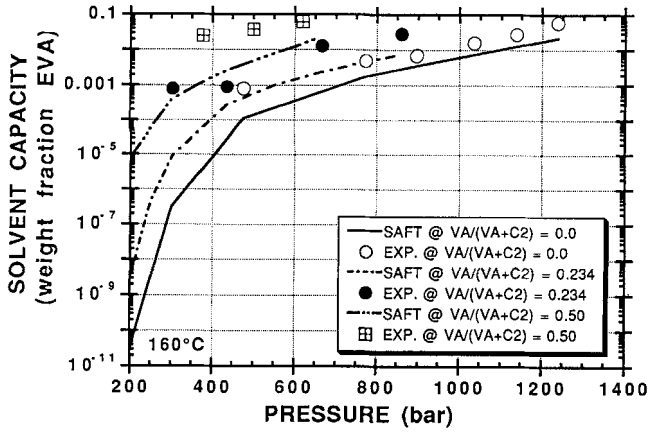

Figure 5. Solvent capacity shown as isopleths as function of pressure.

Continuous curves represent SAFT predictions while points are experimental coexistence data collected in this work. VA weight fraction in solvent mixture (on polymer-free basis) is as indicated in figure legend and temperature is fixed at 160°C.

bar > P > ~ 480 bar) and low temperatures, the free-volume (density) effect is dominant and the solvent capacity decreases with increasing temperature. Note that in the subcritical pressure range (shown qualitatively on the righthand side of Figure 3), where vapor pressure- and enthalpy-related effects are dominant, the solvent capacity increases (due to solute evaporation) with increasing temperature and decreasing pressure (Folie and Radosz, 1995).

The effect of temperature on the ethylene capacity is best illustrated by the isobars shown in Figure 4. Interestingly, SAFT predicts that the ethylene capacity is nearly independent of temperature (in the 130 – 270°C temperature range) at ~ 480 bar. This corresponds to crossover point 1 in Figure 3. At P > ~ 480 bar, the ethylene capacity monotonically increases with temperature. At P < ~ 480 bar, the temperature dependence of the ethylene capacity is nonmonotonic and exhibits a minimum. On the low temperature side,

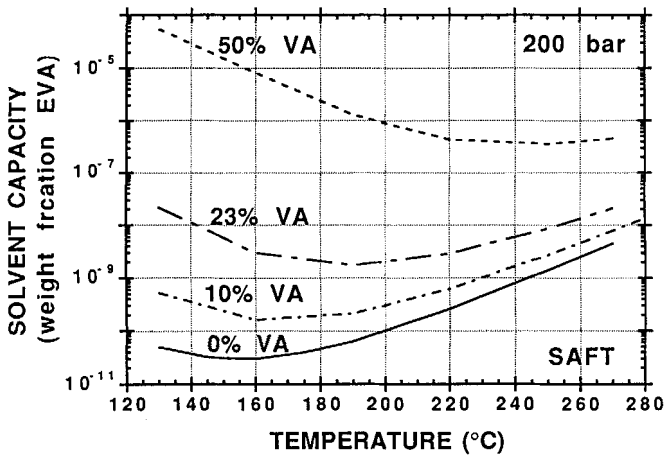

Figure 6. Solvent capacity as predicted by SAFT shown as isopleths as function of temperature.

VA weight percent in solvent mixture (on polymer-free basis) is as indicated in figure legend and pressure is fixed at 200 bar.

where the free-volume (density) effect is dominant, the solvent capacity decreases with increasing temperature. The temperature of that minimum (T_{min}) increases with increasing pressure within the 200 – 300 bar pressure range, as shown in Figure 4.

As pointed out elsewhere (Folie et al., 1996), VA behaves, in general, as a cosolvent to lower the CPP of the EVA-ethylene-VA system. In this work, VA was found to have a similar effect on the solvent capacity. As illustrated in Figure 5, adding VA to solvent mixture in the concentration range 0 – 50 wt. % (on a polymer-free basis) increases the overall solvent capacity at any given pressure, the temperature being fixed in this case at 160°C. At 600 bar, for example, the solvent capacity increases by nearly two orders of magnitude when the VA concentration in the solvent mixture is increased from 0 to 50 wt. %. SAFT correctly predicts this trend as well as the relative increase in solvent capacity, but underestimates somewhat the solvent capacities.

The explanation for the cosolvency effect of VA is threefold. First, the polarizability of VA is twice that of ethylene, which enhances the dispersion forces between the polymer segments and the solvent molecules. Secondly, VA reduces the free-volume of the solvent mixture or, equivalently, increases its density. Third, VA has a permanent dipole moment (1.7 debye), which increases the overall solvent polarity and favors dipole-dipole interactions between VA and the incorporated-VA moieties of the copolymer. As shown elsewhere (Folie et al., 1996), all three effects lead to lower CPPs, hence, to higher polymer solubilities in the PLP.

As shown in Figure 4, the low-pressure isobars behave nonmonotonically with temperature. This nonmonotonic dependence of the solvent capacity on temperature is also illustrated in Figure 6 by isopleths predicted by SAFT at a fixed pressure (200 bar) and at different constant VA concentrations in the solvent mixture (from 0 to 50 wt. % on a polymer-free basis). T_{min} not only increases with increasing pressure (Figure 4), but also with increasing VA concentration in the solvent mixture (Figure 6). Both effects enlarge the temperature range where the free-volume (density) effect is dominant and where the solvent capacity decreases with increasing temperature. For example, with plain ethylene, T_{min} is ~ 150°C, whereas, with 50 wt. % VA in the solvent mixture, T_{min} is ~ 240 °C. It is interesting to note that those changes in the temperature dependence of the solvent capacity brought about by increasing the VA concentration in the solvent mixture correlate well with those observed in the type of fluid → fluid-liquid phase transition. As reported by Folie et al. (1996), the phase behavior of the EVA-ethylene-VA system changes from an upper-solution-temperature-type to a lower-solution-temperature-type upon increasing the VA concentration in the solvent mixture in the temperature range 130 – 250°C.

As illustrated in the previous four figures, the polymer solubility in a supercritical solvent (its capacity) depends, in general, on pressure, temperature, and solvent composition, three independent thermodynamic intensive variables. We found that the solvent capacity is related to the phase densities in a unique way: by plotting the solvent capacity vs. the difference in density between the PRP and the PLP ($\Delta\rho$), all the simulation data collected under the different conditions of temperature, pressure, and solvent composition investigated in

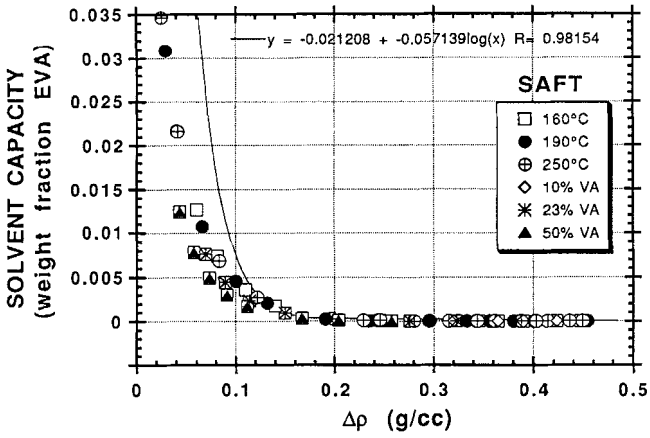

Figure 7. Solvent capacity as predicted by SAFT over broad range of pressure (200 bar to CPP), temperature (160 to 250°C), and VA concentration (0 to 50 wt. %) shown as function of difference in density (also predicted by SAFT) between PRP and PLP.

Data nearly fall onto single master curve which was fitted to function of type: $X' = A + B \log_{10}(\Delta\rho)$, for which constants A and B are indicated in figure.

this work nearly fall on a single master curve. This is shown in Figure 7. As $\Delta\rho$ decreases (such as by increasing pressure), the solvent capacity steadily increases. Note that this increase is very steep when $\Delta\rho$ drops below 0.2 g/mL. Experimental data on the phase densities are required to confirm those simulation results.

Extract yield

In a fractionation process, it is often desirable to know the *extract yield*, defined here as the percentage (in weight) of the parent EVA in the feed extracted by the solvent. The *extract* is therefore the polymer of the PLP, whereas the *raffinate* is the polymer of the PRP. The extract yield (Y) not only depends upon the solvent capacity (X'), but also upon the relative amount of each phase formed according to

$$Y = \left(\frac{X'}{X^F}\right)\left(\frac{r}{r+1}\right) \times 100 \qquad (11)$$

where r, the weight ratio of the PLP to the PRP, can be estimated from the composition of the feed and the coexisting phases according to

$$r = \frac{X'' - X^F}{X^F - X'} \qquad (12)$$

where X^F is the polymer weight fraction in the feed (FEED), X' is the polymer weight fraction in the PLP (= solvent capacity), and X'' is the polymer weight fraction in the PRP.

At the CPP, there are typically two patterns of phase disengagement observed on a macroscopic scale for polymer-SCF systems (Folie and Radosz, 1995). One pattern is similar to a *dew-point* separation in VLE, where one observes the onset and growth of the high-density phase (PRP) upon lowering the pressure below the CPP. The other pattern is similar to a *bubble-point* separation in VLE, where one observes the onset and growth of the low-density phase (PLP) upon

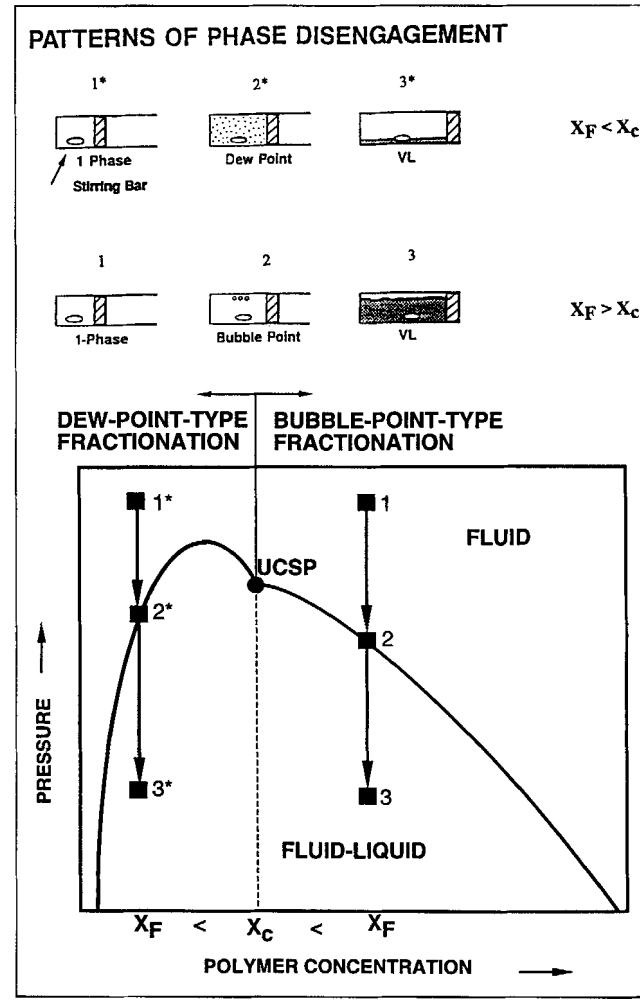

Figure 8. Phase disengagement patterns occurring as pressure is progressively reduced below CPP.

Shaded area represents PRP. As shown by qualitative P-X (pressure-composition) diagram typical for polydisperse polymer-solvent system, dew-point-type fractionation occurs if polymer concentration in feed (X^F) is smaller than critical concentration (X_c), whereas bubble-point-type fractionation occurs if $X^F > X_c$.

lowering the pressure below the CPP. The two different phase transition mechanisms are illustrated in Figure 8. As detailed elsewhere (Folie and Radosz, 1995), a dew-point transition occurs when the polymer concentration in the feed (X^F) is smaller than the critical concentration (X_c), whereas a bubble-point transition occurs when $X^F > X_c$. For a dew-point-type fractionation, $X^F = X'$ (FEED = PLP) at the CPP, hence $Y_{CPP} = 100\%$ since in Eq. 11, $r/(r+1) = 1$ when $r \to \infty$. On the other hand, for a bubble-point-type fractionation $X^F = X''$ (FEED = PRP) at the CPP; hence, $Y_{CPP} = 0\%$ since $r = r/(r+1) = 0$ when $P \to$ CPP. In both cases at low enough pressures, r approaches a constant value equal to the solvent to polymer ratio in the feed, whereas Y becomes vanishingly small, such that $r = (1 - X^F)/X^F$ and $Y = 0\%$ when $P \to 0$.

As illustrated in Figure 9 for the fractionation of 15 wt. % EVA in ethylene at 190°C, Y varies nonmonotonically with pressure for a bubble-point-type fractionation. The maximum Y value occurs close to the CPP where $Y_{CPP} = 0\%$ by definition. The sudden drop in the extract yield near the CPP is

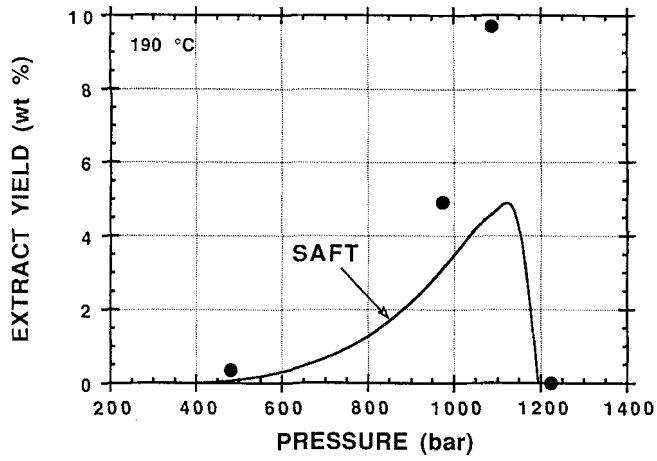

Figure 9. Extract yield (Y) shown as function of pressure at 190°C for typical bubble-point-type fractionation.

Solid curve represents SAFT predictions while points were calculated from Eqs. 11 and 12 with experimental coexistence data collected in this work.

due to the fact that $r/(r+1)$ (= PLP/FEED) in Eq. 11 rapidly decreases towards zero in the vicinity of the CPP, as shown in Figure 10. The SAFT predictions shown in Figures 9 and 10 are in good agreement with the data collected in this work. Y is underpredicted by SAFT near the CPP (Figure 9) because $r/(r+1)$ is underestimated by SAFT in that region (Figure 10).

The effect of the VA cosolvency on the extract yield is illustrated by the experimental data shown in Figure 11 for three bubble-point-type fractionations. Because of its stronger solvating power, VA significantly reduces the pressure required to extract the polymer. For example, ~ 300 bar is sufficient to extract 10 wt. % EVA in the presence of 50 wt. %. VA in the solvent mixture, whereas ~ 1,100 bar is required with plain ethylene. Note that the maximum Y value (20–25%) does not appear to significantly depend on the solvent

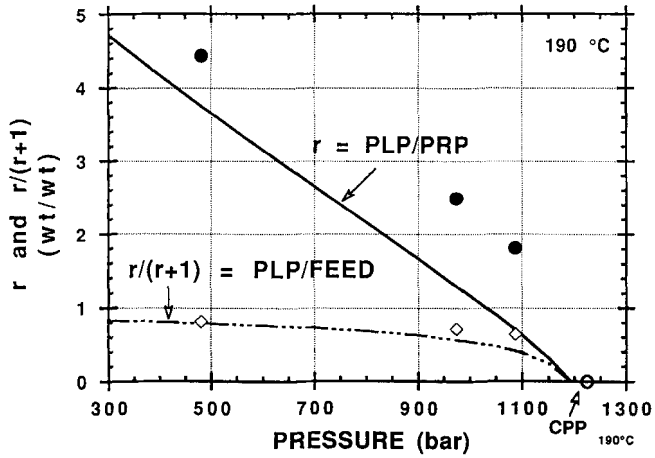

Figure 10. Functional dependence of r and $r/(r+1)$ upon pressure (300 bar to CPP) for typical bubble-point-type fractionation performed at constant temperature of 190°C.

Continuous curves represent SAFT results while points were calculated from Eq. 12 with experimental coexistence data collected in this work.

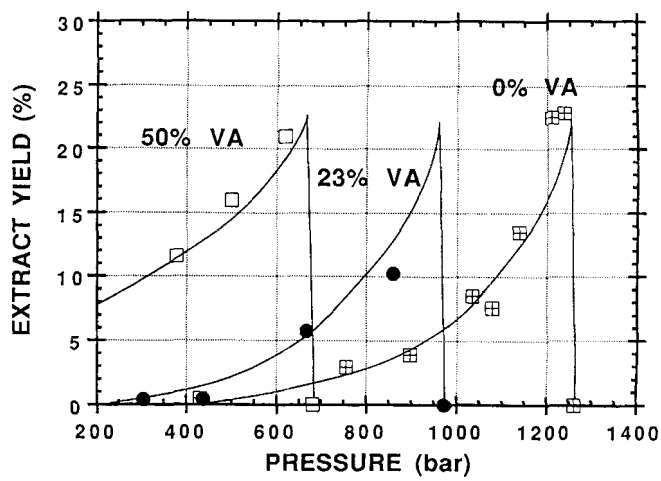

Figure 11. Effect of VA cosolvency on extract yield, shown at three different constant VA concentrations in solvent mixture (on polymer-free basis) and at fixed temperature of 160°C.

Points represent experimental data collected in this work.

composition in the range of concentrations investigated in this work.

SAFT predicts that Y and X' monotonically increase with pressure in the case of a dew-point-type fractionation, as illustrated in Figure 12a for the fractionation of 2 wt. % EVA in ethylene at 190°C. At the CPP, $Y_{CPP} = 100\%$ and $X' = X^F = 0.02$ by definition. Shown in Figure 12b is the functional dependence of r and $r/(r+1)$ upon pressure, as predicted by SAFT, for the same dew-point-type fractionation. Both variables exhibit a nonmonotonic dependence upon pressure with a minimum near 1,200 bar. This nonmonotonic dependence can be explained by the fact that two opposing effects determine the amount of PRP formed; on the one hand, as the pressure decreases, more and more polymer precipitates which tends to lower r and $r/(r+1)$. On the other hand, the ethylene solubility in the PRP decreases as the pressure is reduced which tends to raise r and $r/(r+1)$. As shown in Figure 12b, the former effect is dominant near the CPP, whereas the latter dominates at pressures less than ~ 1,200 bar.

Extract and raffinate

The key to understanding a polymer fractionation process is the ability to predict the changes in the extract and raffinate MW and polydispersity in terms of the process parameters. The effect of pressure and solvent composition, for example, on the extract and raffinate M_n and polydispersity is illustrated in Figures 13 to 16 for a bubble-point-type and a dew-point-type fractionation.

Bubble-Point-Type Fractionation. Shown in Figure 13 are the SAFT predictions of the extract and raffinate M_n resulting from the fractionation of EVA performed at a constant temperature of 190°C and at two different constant solvent compositions, 0 and 50 wt. % VA (on a polymer-free basis). Those results are typical for a bubble-point-type fractionation for the polymer concentration in the feed ($X^F = 0.15$) is greater than the critical concentration (X_c), previously re-

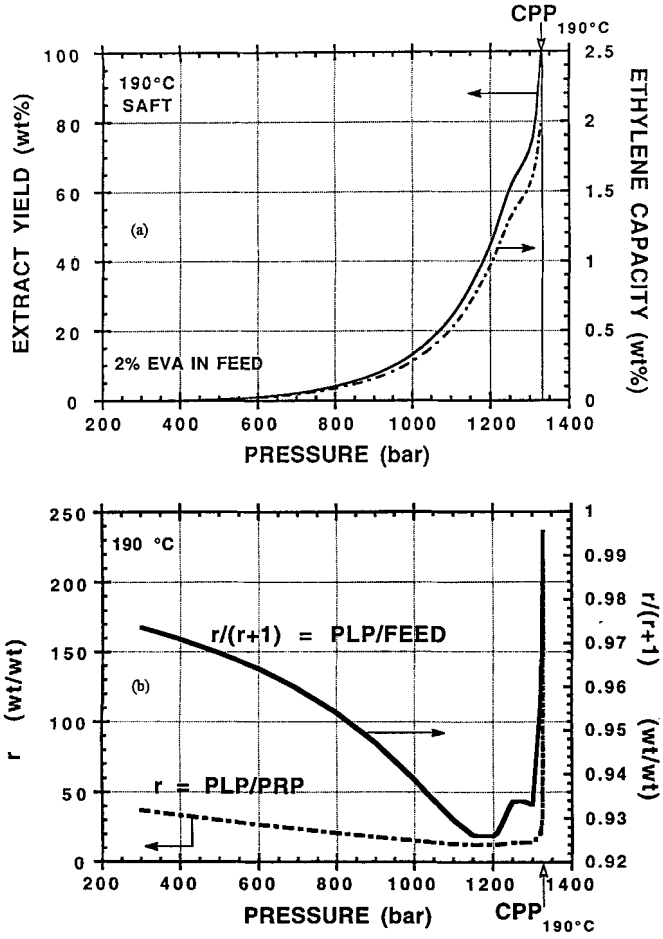

Figure 12. (a) Ethylene capacity and extract yield predicted by SAFT for typical dew-point-type fractionation as function of pressure (300 bar to the CPP) at 190°C; (b) functional dependence of r and $r/(r+1)$ on pressure as predicted by SAFT for the same dew-point-type fractionation.

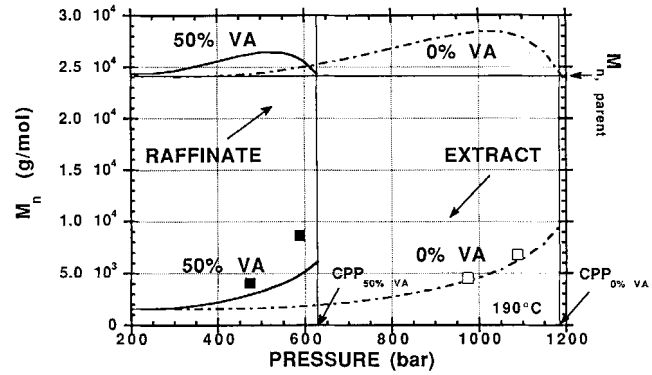

Figure 13. Extract and raffinate M_n as predicted by SAFT for typical bubble-point-type fractionation ($X^F > X_c$), shown as function of pressure (200 bar to CPP) at two different constant VA concentrations in solvent mixture (on polymer-free basis), 0 and 50 wt. %.

Temperature is fixed at 190°C. Continuous curves represent SAFT results while squares correspond to extract M_n measured by SEC.

ported (Folie et al., 1996) to be ~ 0.08 weight fraction for this particular polymer. As indicated by the shape of the two curves shown at the bottom of Figure 13, the extract M_n monotonically increases with increasing pressure from ~ 1.5 kg/mol at 200 bar to ~ 10 kg/mol at the CPP in the VA-free case. In both cases, the SAFT simulation results are in good agreement with the experimental data obtained from the SEC analyses of two extracts.

The raffinate M_n, on the other hand, exhibits a nonmonotonic dependence upon pressure with a maximum value of ~ 28 kg/mol near 1,000 bar in the VA-free case, as shown at the top of Figure 13. Similar trends were reported by Bodganovic et al. (1981, 1985) and Jungermann and Luft (1987) who used, respectively, the Flory-Prigogine free-volume theory and the perturbed-hard-chain theory to simulate the fractionation of a LDPE in ethylene at high pressures. This behavior can be explained by the following arguments. At low pressures (such as 200 bar), the solvent capacity is so small that the raffinate M_n is essentially the same as that of the parent (unfractionated) polymer. As the pressure is increased, both the solvent capacity and the extract yield increase. Since the light ends are preferentially extracted, the raffinate M_n steadily increases with increasing pressure. In the vicinity of the CPP, the abrupt drop in the extract yield (Figure 9) overwhelms the continuous increase in the solvent capacity. The net result is a decrease in the raffinate M_n with increasing pressure in that region. At the CPP, the raffinate M_n is equal to that of the parent polymer ($M_{n,\text{parent}} = 24$ kg/mol). As shown again in Figure 13, VA acts as a cosolvent to reduce the CPP from 1,190 bar to 630 bar when the VA concentration in the solvent mixture is increased from 0 to 50 wt. %. Since adding VA to the solvent mixture raises the solvent density and lowers its selectivity, the extract and raffinate M_n increase with increasing VA concentration in the solvent mixture.

As shown in Figure 14, SAFT predicts that the extract and raffinate polydispersity (M_w/M_n) exhibits the same characteristic pressure dependence than M_n. The extract polydispersity monotonically increases with pressure, whereas raffinate polydispersity varies nonmonotonically with pressure, exhibiting a minimum of ~ 3.7 near 1,000 bar in the VA-free case. This represents a 14% decrease in polydispersity relative to that of the parent material ($M_w/M_n = 4.30$). Note that these simulations were performed with eight pseudocomponents (Table 1) in order to reduce the computational time. This explains why the polydispersity of the parent EVA is slightly larger than that measured by SEC ($M_w/M_n = 3.35$). The increase in the extract polydispersity with pressure can be understood by the fact that the density of the solvent, hence its capacity, increases with pressure. As pointed out by Chen et al. (1993, 1994a), this makes the solvent less selective, that is to say, capable of solvating EVA molecules of very different chain lengths. At low pressures (< 250 bar), SAFT predicts that the extract becomes nearly monodisperse (in fact, it is equal to the polydispersity of the lowest-MW pseudocomponent, EVA1, which is 1.027 as indicated in Table 1). Note that even at pressures approaching the CPP, the extract polydispersity is only about 2.0 (in good agreement with the experimental data shown in Figure 14), which is small comparatively to the polydispersity of the parent EVA. Because of the

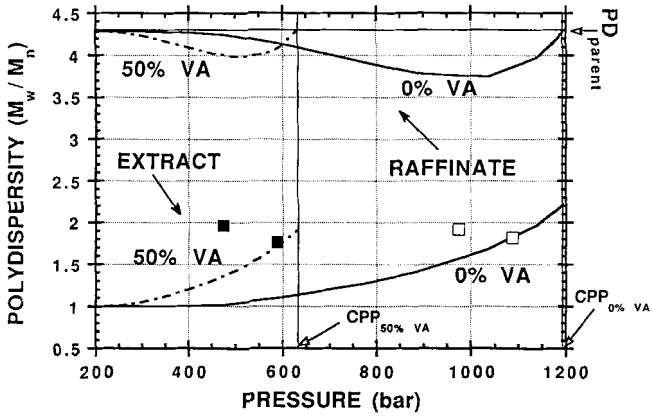

Figure 14. Extract and raffinate polydispersity (abbreviated as PD) as predicted by SAFT for typical bubble-point-type fractionation ($X^F > X_c$), shown as function of pressure (200 bar to CPP) at two different constant VA concentrations in solvent mixture (on polymer-free basis), 0 and 50 wt. %.

Temperature is fixed at 190°C. Continuous curves represent SAFT results while squares correspond to extract polydispersity measured by SEC.

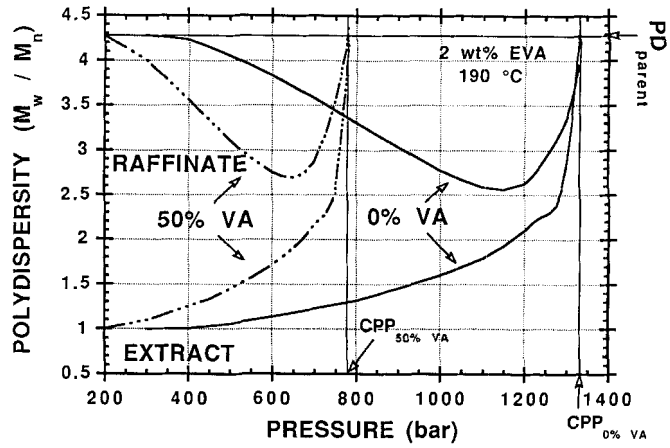

Figure 16. Extract and raffinate polydispersity (abbreviated as PD) as predicted by SAFT for typical dew-point-type fractionation ($X^F < X_c$) as a function of pressure (200 bar to the CPP) at two different constant VA concentrations in solvent mixture (on polymer-free basis), 0 and 50 wt. %.

Temperature is fixed at 190°C.

VA cosolvency effect, the extract polydispersity increases whereas the raffinate polydispersity decreases with increasing VA concentration in the solvent mixture.

Dew-Point-Type Fractionation. Shown in Figure 15 are SAFT predictions of the extract and raffinate M_n resulting from the dew-point-type fractionation of EVA performed at a constant temperature of 190°C and at two different constant solvent compositions, 0 and 50 wt. % VA (on a polymer-free basis). In this case, the polymer concentration in the feed ($X^F = 0.02$) is smaller than the critical concentration ($X_{crt} \approx 0.08$). As in the case of the bubble-point-type fractionation, the extract M_n monotonically increases with pressure. This is related to the fact that both the extract yield and the solvent capacity monotonically increase with pressure (Figure 12a). In this case, however, the extract M_n is equal to

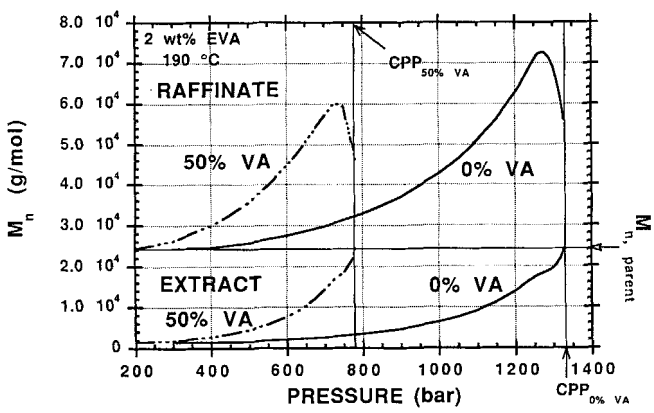

Figure 15. Extract and raffinate M_n as predicted by SAFT for typical dew-point-type fractionation ($X^F < X_c$) as function of pressure (200 bar to CPP) at two different constant VA concentrations in solvent mixture (on polymer-free basis), 0 and 50 wt. %.

Temperature is fixed at 190°C.

$M_{n,parent}$ at the CPP. The raffinate M_n exhibits again a nonmonotonic dependence upon pressure, with a maximum value near the CPP (~ 72 kg/mol in the VA-free case shown in Figure 15) much larger than $M_{n,parent}$. This results from the fact that it is the heavy ends which precipitate first from solution to form the dispersed phase (PRP) as the pressure is reduced below the CPP.

The SAFT predictions of the extract and the raffinate polydispersity for the same dew-point-type fractionation are shown in Figure 16. Similarly to what was observed for the bubble-point-type fractionation (Figure 14), the polymer polydispersity in both phases is less than that of the parent EVA, as reported elsewhere (Kang and Sandler, 1988; Kang et al., 1989; Spahl and Luft, 1983). Those simulation results also indicate that under identical operating conditions a dew-point-type fractionation is more efficient than a bubble-point-type fractionation to raise the raffinate M_n and to reduce its polydispersity. This, in fact, represents the basis for separation by fractional precipitation from a dilute polymer solution, as explained by Flory (1990). Adding VA as a cosolvent decreases the pressure required to lower the raffinate polydispersity. For example, the pressure necessary to lower the raffinate polydispersity from 4.3 to ~ 2.7 is ~ 650 bar with 50 wt. % VA in the solvent mixture, whereas ~ 1,050 bar is required with plain ethylene.

The extract and raffinate M_n and polydispersity also depend on the temperature and the polymer concentration in the feed (X^F). SAFT predicts that, for this particular system, increasing the temperature in the range of 130 to 250°C has the same effect on the extract and raffinate M_n and polydispersity than increasing the VA concentration in the solvent mixture (results not shown). This is in agreement with the observations made by Spahl and Luft (1983) who reported that both the extract and raffinate M_n and M_w increase with increasing temperature in the range 110 to 200°C for a LDPE fractionated in ethylene by a dew-point-type fractionation. In general, the extract and raffinate MW decrease with increas-

ing X^F, as observed by Luft and Lindner (1976) and Bogdanovic et al. (1981, 1985).

Conclusion

The single-stage fractionation of a commercial polydisperse EVA in supercritical ethylene and ethylene-VA mixtures is modeled with the SAFT EOS coupled to a block-algebra flash algorithm developed for large multicomponent systems. The polymer MWD measured by SEC is optimally represented by ten nearly-monodisperse pseudocomponents in these simulations. By using only three MW- and temperature-independent binary interaction parameters (k_{ij}s) previously determined from VLE and cloud point data, SAFT is found to account quantitatively for the effect of pressure, temperature, and VA concentration in the solvent mixture on the fractionation process over a broad range of conditions.

Acknowledgments

We gratefully acknowledge the assistance of Pr. M. Radosz (Louisiana State University, Baton Rouge, LA) for providing the multicomponent flash algorithm, Pr. G. Luft (Technische Hochschule Darmstadt, Germany) for performing the phase equilibrium experiments, and Dr. G. Steenbeke (Exxon Chemical Europe, Belgium) for performing the SEC analyses. A preliminary account of this work was presented at the AIChE Meeting, Miami Beach, FL, Nov. 12–17, 1995.

Literature Cited

Banaszak, M., Y. C. Chiew, and M. Radosz, "Thermodynamic Perturbation Theory: Sticky Chains and Square-Well Chains," *Phys. Rev. E*, **48,** 3760 (1993).

Bogdanovic, V., A. Tasic, and B. Djordjevic, "Phase Equilibrium Calculations for Ethylene-Multicomponent Polyethylene Mixtures at High Pressures," *Fluid Phase Equilib.*, **6,** 83 (1981).

Bogdanovic, V., B. Djordjevic, and A. Tasic, "Phase Separation in the Ethylene-Polyethylene System at High Pressures. V. The Calculation of Equilibrium Data for the Pressure Range 100–300 MPa," *J. Serb. Chem. Soc.*, **50,** 557 (1985).

Bolanos, G., and M. C. Thies, "Supercritical Toluene-Petroleum Pitch Mixtures: Liquid-Liquid Equilibria and SAFT Modeling," *Proc. Int. Conf. on Fluid Properties and Phase Equilibria for Chemical Process Design*, Snowmass, CO, 603 (June 18–23, 1995).

Bonner, D. C., D. P. Maloney, and J. M. Prausnitz, "Calculation of High-Pressure Phase Equilibria and Molecular-Weight Distribution in Partial Decompression of Polyethylene-Ethylene Mixtures," *Ind. Eng. Chem. Process Des. Dev.*, **13,** 91 (1974).

Chapman, W. G., K. E. Gubbins, G. Jackson, and M. Radosz, "New Reference Equation of State for Associating Liquids," *Ind. Eng. Chem. Res.*, **29,** 1709 (1990).

Chen, C.-k., M. A. Duran, and M. Radosz, "Two-Phase Equilibria in Asymmetric Polymer Solutions; Block-Algebra, A New Flash Algorithm Coupled with SAFT Equation of State, Applied to Single-Stage Dual Solvent Supercritical Fractionation of Polyethylene," *Ind. Eng. Chem. Res.*, **32,** 3123 (1993).

Chen, C.-k., M. A. Duran, and M. Radosz, "Supercritical Antisolvent (SAS) Fractionation of Polyethylene Simulated with Multistage Algorithm and SAFT Equation of State: Staging Leads to High Selectivity Enhancements for Lights," *Ind. Eng. Chem. Res.*, **33,** 306 (1994a).

Chen, S.-j., Y. C. Chiew, J. A. Gardecki, S. Nilsen, and M. Radosz, "P-V-T Properties of Alternating Poly(Ethylene-Propylene) Liquids," *J. Poly. Sci.: Part B: Poly. Phys.*, **32,** 1791 (1994b).

Cotterman, R. L., and J. M. Prausnitz, "Flash Calculations for Continuous or Semicontinuous Mixtures Using an Equation of State," *Ind. Eng. Chem. Process Des. Dev.*, **24,** 434 (1985).

Finck, U., C. Wohlfarth, and T. Heuer, "Calculation of High Pressure Phase Equilibria of Mixtures of Ethylene, Vinyl Acetate, and an (Ethylene-Vinyl Acetate) Copolymer," *Ber. Bunsenges. Phys. Chem.*, **96,** 179 (1992).

Flory, P. J., *Principles of Polymer Chemistry*, Cornell University Press, Ithaca, NY (1990).

Folie, B. J., and M. Radosz, "Phase Equilibria in High-Pressure Polyethylene Technology," *Ind. Eng. Chem. Res.*, **34,** 1501 (1995).

Folie, B. J., C. Gregg, G. Luft, and M. Radosz, "Phase Equilibria of Poly(ethylene-co-vinyl acetate) in Subcritical and Supercritical Ethylene and Ethylene-Vinyl Acetate Mixtures," *Fluid Phase Equilib.*, **120,** 11 (1996).

Gregg, C. J., S.-j. Chen, F. P. Stein, and M. Radosz, "Phase Behavior of Binary Ethylene-Propylene Copolymer Solutions in Sub- and Supercritical Ethylene and Propylene," *Fluid Phase Equilib.*, **83,** 375 (1993).

Gregg, C. J., F. P. Stein, and M. Radosz, "Phase Behavior of Telechelic Polyisobutylene (PIB) in Subcritical and Supercritical Fluids: I. Inter- and Intra-Association Effects for Blank, Monohydroxy, and Dihydroxy PIB(1K) in Ethane, Propane, Dimethyl Ether, Carbon Dioxide, and Chlorodifluoromethane," *Macromol.*, **27,** 4972 (1994).

Hasch, B. M., E. J. Maurer, L. F. Ansanelli, and M. A. McHugh, "(Methanol + Ethene): Phase Behavior and Modeling with the SAFT Equation of State," *J. Chem. Thermodynamics*, **26,** 625 (1994).

Huang, S. H., and M. Radosz, "Equation of State for Small, Large, Polydisperse, and Associating Molecules," *Ind. Eng. Chem. Res.*, **29,** 2284 (1990).

Huang, S. H., and M. Radosz, "Equation of State for Small, Large, Polydisperse, and Associating Molecules: Extension to Fluid Mixtures," *Ind. Eng. Chem. Res.*, **30,** 1994 (1991a).

Huang, S. H., and M. Radosz, "Phase Behavior of Reservoir Fluids III: Molecular Lumping and Characterization," *Fluid Phase Equilib.*, **66,** 1 (1991b).

Huang, S. H., and M. Radosz, "Phase Behavior of Reservoir Fluids IV: Molecular-Weight Distributions for Thermodynamic Modeling," *Fluid Phase Equilib.*, **66,** 23 (1991c).

Jungermann, G., and G. Luft, "Vergleich der Perturbed-Hard-Chain-Theorie mit der Freien-Volumen-Theorie und der Flory-Huggins-Theorie zur Berchnung von Phasengleichgewichten von Ethylen/Polyethylen-Mischungen unter Hochdruch," *Ber. Bunsenges. Phys. Chem.*, **91,** 541 (1987).

Kang, C. H., and S. I. Sandler, "Effects of Polydispersity on the Phase Behavior of Aqueous Two-Phase Polymer Systems," *Macromol.*, **21,** 3088 (1988).

Kang, C. H., C-K. Lee, and S. I. Sandler, "Polydispersity Effects on the Behavior of Aqueous Two-Phase Two-Polymer Systems," *Ind. Eng. Chem. Res.*, **28,** 1537 (1989).

Koningsveld, R., and A. J. Staverman, "Liquid-Liquid Phase Separation in Multicomponent Polymer Solutions. I. Statement of the Problem and Description of Methods of Calculation," *J. of Poly. Sci., A-2*, **6,** 305 (1968).

Lee, S-H., M. A. LoStracco, and M. A. McHugh, "High-Pressure, Molecular Weight-Dependent Behavior of (Co)polymer-Solvent Mixtures: Experiments and Modeling," *Macromol.*, **27,** 4652 (1994).

Liu, D. D., and J. M. Prausnitz, "Calculation of Phase Equilibria for Mixtures of Ethylene and Low-Density Polyethylene at High Pressures," *Ind. Eng. Chem. Process Des. Dev.*, **19,** 205 (1980).

Luft, G., and A. Lindner, "Zum Einfluss Polymermolekulargewichts auf das Phasenverhalten von Gas-Polymer-Systemen unter Hochdruck," *Angew. Makro. Chem.*, **56,** 99 (1976).

Luft, G., and N. S. Subramanian, "Phase Behavior of Mixtures of Ethylene, Methyl Acrylate, and Copolymers under High Pressures," *Ind. Eng. Chem. Res.*, **26,** 750 (1987).

Ratzsch, M. T., P. Wagner, C. Wohlfarth, and S. Gleditzsch, "Untersuchungen zum Hochdruckphasengleichgewicht in Mischungen aus Ethylen und (Ethylen-Vinylacetat)-Copolymeren," *Acta Polymerica*, **34,** 340 (1983).

Sako, T., A. H. Wu, and J. M. Prausnitz, "A Cubic Equation of State for High-Pressure Phase Equilibria of Mixtures Containing Polymers and Volatile Fluids," *J. Appl. Poly. Sci.*, **38,** 1839 (1989).

Spahl, R., and G. Luft, "Fraktionierungserscheinungen bei der Entmischung von Ethylen-Polyethylen-Gemischen," *Angew. Makro. Chem.* **115,** 87 (1983).

Wohlfarth, C., "Calculation of Phase Equilibria in Random Copolymer Systems," *Makromol. Chem. Theory Simul.*, **2,** 605 (1993).

Manuscript received Oct. 18, 1995, and revision received May 13, 1996.